RAA 2021 Vol. **21** No. **3**, 76(10pp) doi: 10.1088/1674-4527/21/3/76

http://www.raa-journal.org *http://iopscience.iop.org/raa*

Research in Astronomy and Astrophysics

FUV and NIR size of the HI selected low surface brightness galaxies

Cheng Cheng[1], Wei Du[2,3], Cong Kevin Xu[1], Tian-Wen Cao[1], Hong-Xin Zhang[4,5], Jia-Sheng Huang[1], Chuan He[1], Zi-Jian Li[1], Shu-Mei Wu[1], Hai Xu[1], Y. Sophia Dai[1], Xu Shao[1] and Marat Musin[1]

[1] Chinese Academy of Sciences South America Center for Astronomy, National Astronomical Observatories, CAS, Beijing 100101, China; *chengcheng@nao.cas.cn*
[2] National Astronomical Observatories, Chinese Academy of Sciences, Beijing 100101, China
[3] Key Laboratory of Optical Astronomy, NAOC, 20A Datun Road, Chaoyang District, Beijing 100101, China
[4] CAS Key Laboratory for Research in Galaxies and Cosmology, Department of Astronomy, University of Science and Technology of China, Hefei 230026, China
[5] School of Astronomy and Space Science, University of Science and Technology of China, Hefei 230026, China

Received 2020 June 16; accepted 2020 August 25

Abstract How low surface brightness galaxies (LSBGs) form stars and assemble stellar mass is one of the most important questions related to understanding the LSBG population. We select a sample of 381 HI bright LSBGs with both far ultraviolet (FUV) and near infrared (NIR) observations to investigate the star formation rate (SFR) and stellar mass scales, and the growth mode. We measure the FUV and NIR radii of our sample, which represent the star-forming and stellar mass distribution scales respectively. We also compare the FUV and H band radius-stellar mass relation with archival data, to identify the SFR and stellar mass structure difference between the LSBG population and other galaxies. Since galaxy HI mass has a tight correlation with the HI radius, we can also compare the HI and FUV radii to understand the distribution of HI gas and star formation activities. Our results show that most of the HI selected LSBGs have extended star formation structure. The stellar mass distribution of LSBGs may have a similar structure to disk galaxies at the same stellar mass bins, but the star-forming activity of LSBGs happens at a larger radius than the high surface density galaxies, which may help to identify the LSBG sample from the wide-field deep u band image survey. The HI is also distributed at larger radii, implying a steeper (or not) Kennicutt-Schmidt relation for LSBGs.

Key words: Galaxies: evolution — Galaxies: dwarf — Ultraviolet: galaxies — Galaxies: star formation

1 INTRODUCTION

Low surface brightness galaxies (LSBGs) are attracting more and more attention in studies of galaxy formation and evolution. This is not only because they are mainly young galaxies with a faint and diffuse nature, which might provide clues to galaxy formation, but also because of their interesting connection with their dark matter halos (Impey & Bothun 1997; Bothun et al. 1997).

Traditionally, LSBGs are selected by the centre surface brightness of a galaxy in B band (McGaugh 1996). Since B band is more sensitive to star formation, such selection of the LSBG sample may cause a bias in the galaxy population with a diffuse star formation structure. Moreover, an average LSBG has a relatively young stellar population and low metallicity (Du et al. 2017). The typical stellar mass is much lower than M^* at a similar redshift (Du et al. 2020), indicating an early forming stage of the galaxies.

However, due to their low surface brightness nature, it is difficult to obtain an optical spectrum with enough signal to noise ratio even to identify the redshifts (van Dokkum et al. 2015; Greco et al. 2018b,a). Thus a large sample of LSBGs with reliable redshifts is still quite scant, limiting the statistical study of LSBGs. Luckily, most LSBGs are low mass galaxies, which tend to be rich in HI (Huang et al. 2012; Maddox et al. 2015), so wide field HI survey projects such as Arecibo Legacy Fast ALFA (ALFALFA) (Haynes et al. 2011, 2018), combined with Sloan Digital Sky Survey (SDSS) optical images, could provide us optimal means to obtain a large sample of LSBGs with reliable HI redshift. Our previous series of studies based on the LSBGs selected from the ALFALFA sample with optical surface brightness measured from SDSS images (Du et al. 2015; He et al.

2019; Du et al. 2019) has shown that LSBGs have much lower metallicity (Du et al. 2017), follow the Tully-Fisher relation (Du et al. 2019) and have similar mass-light ratios as high surface brightness galaxies (Du et al. 2020). The Hα images of our HI selected LSBG sample also confirm that the star formation surface density has a very weak correlation with the gas surface density, and the star formation surface density is much lower than the prediction from the Kennicutt-Schmidt law (Kennicutt 1998; Kennicutt & Evans 2012), leading to significantly longer gas depletion time scales, and low star formation efficiency (Lei et al. 2018, 2019).

Although a typical LSBG is rich in neutral hydrogen gas, the star formation rate (SFR) is not high. For one thing, LSBGs are located in the lower stellar mass end of the star forming galaxy main sequence, where the SFR is lower. The other cold H_2 gas, which is the direct fuel of star formation, is rarely detected in LSBGs. Moreover, the transition from HI to H_2 may also have very low efficiency in a low metallicity environment (Omukai et al. 2005; Glover & Clark 2012). H_2 gas forms on the surface of dust grains (Hollenbach & McKee 1979) and requires high gas density (Leroy et al. 2008), but LSBGs have short star formation history, and thus may not be able to accumulate enough dust. The extended morphology also implies the HI gas is not concentrated in the galaxy centre (Cao et al. 2017).

Study of star formation in LSBGs is crucially important to understanding the formation process in the young galaxy population with extreme properties such as low mass, low dust and low metallicity. One simple and yet fundamental parameter that can be utilized to investigate galaxy formation and the related evolution path is the galaxy size in different bands (Cheng et al. 2020). Previous studies indicate that massive star-forming galaxies have a larger star formation radius than that of the stellar distribution radius, implying an "inside-out" growth mode because most of the stars are concentrated in the galaxy's central region, but star formation is more extended (Kelvin et al. 2012). Since near infrared (NIR) bands trace the flux from the old stellar population, which possesses the majority of stellar mass, it can be used to trace the stellar mass distribution, especially for low mass galaxies (Suess et al. 2019a,b). On the other hand, SFR radius can be derived from several spatially resolved indicators originating from the young stellar population emission, or re-radiation, such as ultraviolet (UV) and far infrared (FIR) broadband images, the Hα map from narrowband images or integral field unit (IFU) observations. Each SFR indicator has its own advantage, but most of them suffer from the issue of dust extinction. Since LSBGs have low dust abundance (e.g., the $g - r$ colour in Du et al. 2015), far ultraviolet (FUV) images might be the simplest method to reveal the SFR distribution and to estimate the star formation radius.

By comparing the UV and NIR band Hubble Space Telescope (HST) images in the GOODS-North field, we have found that low mass star-forming galaxies can have an "outside-in" growth mode, which means that star formation is active in the galaxy centre, but the stars already formed at a larger radius (Cheng et al. 2020). Nevertheless, our previous results based on HST images only covered UV bright galaxies with optical spectroscopy redshift, which usually have a high central surface brightness. LSBGs, as influential members of the low mass galaxy population, are absent in Cheng et al. (2020). So in this work, we select a sample of HI bright LSBGs with GALEX and UKIRT detection, aiming to study the growth mode of LSBGs.

Throughout this paper, we assume a standard ΛCDM cosmology with $H_0 = 70\,\mathrm{km\,s^{-1}\,Mpc^{-1}}$, $\Omega_{\rm M} = 0.3$ and $\Omega_\Lambda = 0.7$. All the magnitudes are in the AB magnitude system (Oke & Gunn 1983).

2 SAMPLE SELECTION

Our previous work (Du et al. 2015) compiled a sample of 1129 LSBGs with HI detected by the Arecibo telescope, which is the parent sample of this work. The HI selection enables us to have the spec-z of galaxies fainter than what is available from the SDSS spec-z, and reach a low stellar mass galaxy population. We select the LSBGs based on the classical criterion that B band central surface brightness $\mu_{0,\rm B} > 22.5\,\mathrm{mag\,arcsec^{-2}}$. The galaxy's central brightness is derived from the SDSS g, r band images by GALFIT (Peng et al. 2002, 2010a) and calibrated to the B band (Smith et al. 2002). The follow up multi-wavelength study shows that 544 LSBGs in our sample have both GALEX and UKIRT observations (Du et al. 2020). We further remove the galaxies that have a bright neighbour within $2\times R_{\rm optical}$, and remove the galaxies at the edge of the GALEX or UKIRT images. We also remove galaxies with no GALEX FUV detections because this work aims to focus on the properties of star-forming LSBGs. Our final sample contains 381 galaxies. The stellar mass measured from the multi-wavelength catalogue has been presented in Du et al. (2020). We adopt the galaxy distance given by the ALFALFA catalogue.

LSBGs are mainly a population of low mass galaxies. To understand the LSBG properties in a wider picture, we compare the LSBG sample with the low mass galaxy sample in Cheng et al. (2020), which includes galaxies at $0.05 < z_{\rm spec} < 0.3$, $F606W < 24$ AB mag in the Cosmic Assembly Near-infrared Deep Extragalactic Legacy Survey (CANDELS, Grogin et al. 2011; Koekemoer et al. 2011) GOODS-North field (Barro et al. 2019) with a stellar-mass range $10^7 < M_*/M_\odot < 10^{11.4}$. The CANDELS GOOD-North field has been covered by the

Hubble Deep UV Legacy Survey (HDUV, Oesch et al. 2018) in F275W, F336W band. The high spatial resolution of this low-z low mass sample should include more high surface brightness galaxies, for which the spec-z is easier to measure (for more details, see Cheng et al. 2020). We also compare our sample with the low redshift spatially resolved galaxy sample in Trujillo et al. (2020). This sample includes 1005 galaxies with a stellar-mass range of $10^7 < M_*/M_\odot < 10^{12}$ at $z < 0.09$, including various galaxy morphologies. The multi-wavelength spatial resolution and large stellar mass range enable us to compare the LSBG H band radius and analyse the possible origin of the offsets (if any) between the samples. To understand the stellar mass – radius relation of LSBGs and other stellar systems, we also compare our results with Misgeld & Hilker (2011), including stellar systems that span 10 orders of magnitude in mass. Recent results of the Ultra Deep Survey (UDS) sample are also included in this work (van Dokkum et al. 2015; Barbosa et al. 2020).

3 DATA REDUCTION

Resolution of the GALEX FUV image is about 5 arcsec. The star formation regions in the galaxy disk are clumpy, so the FUV images are not as smooth as the optical images with current resolution. Since we only need a rough FUV scale estimation, we convolve the FUV image with a Gaussian kernel that decreases the FUV image spatial resolution to 7 arcsec, 10 arcsec and 15 arcsec full width at half maximum (FWHM). Then we measure the half-light radius with SExtractor individually [1]. We add 1σ noise to the FUV image and measure the half-light radius again to estimate the uncertainty. Since the convolution would smooth the noise and give a smaller uncertainty for the radius, we compare the radius measured from a different kernel convolved image and conclude the scatter of the FUV radius is about 0.05 kpc.

As a consistency check, we also derive the growth curve of the Gaussian kernel convolved FUV image, which is the aperture flux from a series of radii with the centre given by SExtractor. These two methods give consistent results. But since large aperture photometry (at least $5''$ for FUV images) would include more noise, and the background for aperture photometry within the large aperture is not uniform, aperture photometry would underestimate the uncertainty caused by large aperture background estimation. Photometry by SExtractor can estimate the large scale background based on the whole image, and thus would provide more accurate photometry results and better half-light radius results.

Star formation in a galaxy happens discretely. The UV morphology would be very clumpy, which would mislead the source extraction and radius measurements. We convolve this kind of image by a kernel larger than the GALEX point spread function (PSF), which concentrates the UV emission and smooths the UV flux. However, the convolution would involve noise from a nearby source. Moreover, for large galaxies with clumpy FUV morphology, it is also hard to identify whether the clumps at large radii are also part of the central galaxy or objects in the line of sight. In this work, the LSBG FUV images are extended and clumpy. To minimize the effect on the radius measurement, we select our sample with no nearby galaxies within 2 times the optical radius. On the other hand, an LSBG with very clumpy and extended FUV morphology should have a larger half-light radius, and thus a large star formation size, which does not change the main conclusion of this work.

Besides the above non-parametric method, we also fit the GALEX FUV images with a single Sersic function to measure the half-light radius. We adopt the r band galaxy image centre RA, Dec as the centre of the FUV image, which will help us to remove the uncertainty of FUV image centre that is caused by the FUV clumps. We fit the FUV images by GALFIT (Peng et al. 2002, 2010a), which has proved to be one of the standard tools to analyse galaxy morphology. We depict the FUV half-light radius derived from GALFIT and the direct measurement results in Figure 2. The two radii display good consistency, with a typical scatter of about 0.5 kpc.

We utilize SExtractor to estimate the half-light radius. We de-convolve the half-light radius by the relation: $R^2_{\rm half-light} = R^2_{\rm measured-size} - R^2_{\rm PSF-size}$. We regard the galaxies with $R_{\rm measured-size} < R_{\rm PSF-size}$ as unresolved, then we set $R_{\rm PSF-size}$ as the upper limits of the targets. Figure 1 shows one example of the measurement process. The left panel is the FUV image while the right panel features the FUV image that is convolved to $7''$ resolution. The UKIRT H band image has a resolution of about 1 arcsec, which is much lower than the FUV image. We convolve the H band image to 3 to 7 arcsec FWHM, and measure the H band half-light radius following the same method as the FUV radius measurement. We get 312 LSBGs that are resolved in the FUV images and 284 LSBGs that are resolved in H band images. There are 253 LSBGs that have been resolved in both FUV and H bands.

Figure 3 plots the histogram for the radii of our targets in FUV and H bands. The FUV radii of our sample are a bit larger than the H band radii. The upper limits on the radii of the targets that are unresolved in the images are traced by dotted lines. The upper limit on the size of the LSBGs has a wide range in the unit of kpc.

We fit the SED by fastpp[2] (Kriek et al. 2009) with the distance given by ALFALFA, and the SED produced in Du et al. (2020). We employ the Bruzual & Charlot (2003)

[1] GALEX images of our LSBG sample are very clumpy, so SExtractor would treat the clumps as several targets. We decrease the image resolution so that SExtractor can treat the galaxy as one target.

[2] *https://github.com/cschreib/fastpp*

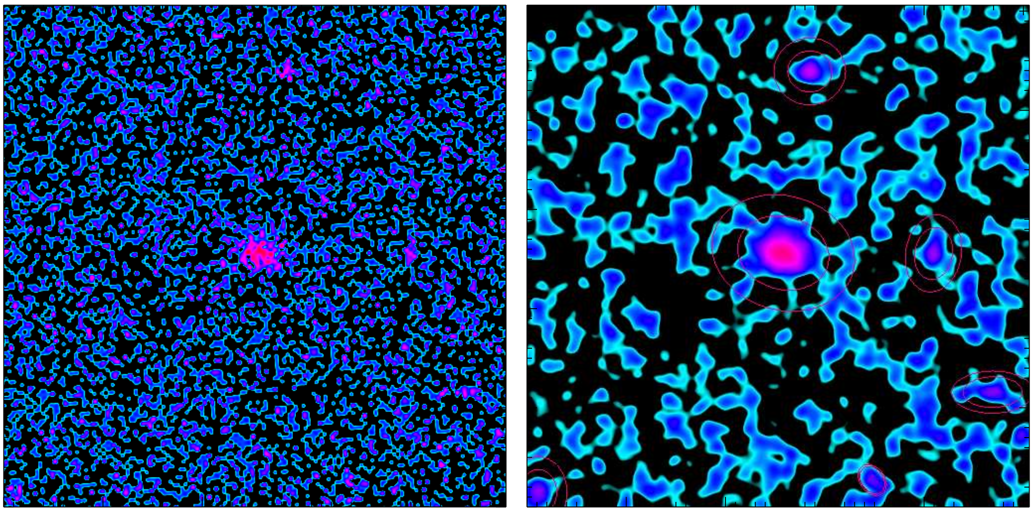

Fig. 1 Example of the radius measurements in FUV images on the scale of $200'' \times 200''$. The *left* panel displays one example of an LSBG, which exhibits a clumpy morphology. We convolve the *left* panel image to a resolution of 7 arcsec in the *right* panel. The morphology of this galaxy is then more concentrated to the centre. Subsequently, we apply SExtractor to measure the half-light radius in the convolved image, and de-convolve the radius by $r^2_{\rm intrinsic} = r^2_{\rm measure} - r^2_{\rm PSF}$. Galaxies with a measured radius larger than $r_{\rm PSF}$ are treated as unresolved targets and will only give upper limits.

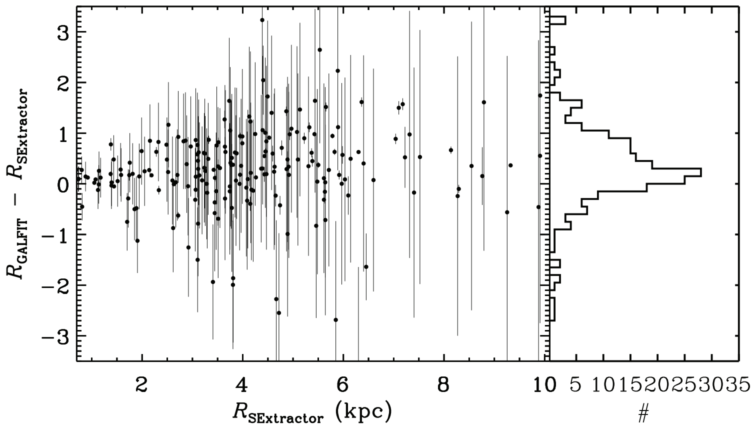

Fig. 2 Distribution of the FUV half light radius difference between $R_{\rm SExtractor}$ from the non-parametric method (SExtractor) and $R_{\rm GALFIT}$ from the parametric method (GALFIT). The two methods show consistent results, with a typical scatter of about 0.5 kpc.

stellar population synthesis models (BC03), and choose the Chabrier initial mass function (IMF) (Chabrier 2003). We also adopt the Calzetti et al. (2000) dust extinction law with attenuation in the range of $0 < Av < 3$. The uncertainty in the stellar mass fitting results is about 0.5 dex.

4 RESULTS

We compare the FUV band radius of our LSBG sample with the galaxy FUV size from GALEX Nearby Galaxies Survey (NGS, at z ∼0 Gil de Paz et al. 2007) with the latest stellar mass measurements from the z = 0 Multi-wavelength Galaxy Synthesis (z0MGS) project (Leroy et al. 2019) in Figure 4. We also show the CANDELS GOODS-North F275W band half-light radius from Cheng et al. (2020). The LSBGs exhibit a higher FUV radius, indicating a more extended star formation region than most of the local UV bright galaxies with the same stellar mass range. We also colour the NGS sample with the morphology type T to highlight the morphology trend and discuss the FUV size in Section 5.3.

The H band size vs. stellar-mass relation is plotted in Figure 5. Since the half mass radius and half-light radius ratio for the galaxies with about $10^9\,M_\odot$ stellar mass is about $0.8 - 1$ (e.g., the fig. 1 in Suess et al. 2019b), we can compare our half-light radius of the LSBGs in H band with the previous half mass radius results in Trujillo et al. (2020), which include a sample of 1005 galaxies that spans five orders of magnitude in stellar mass ($10^7 < M_*/M_\odot <$

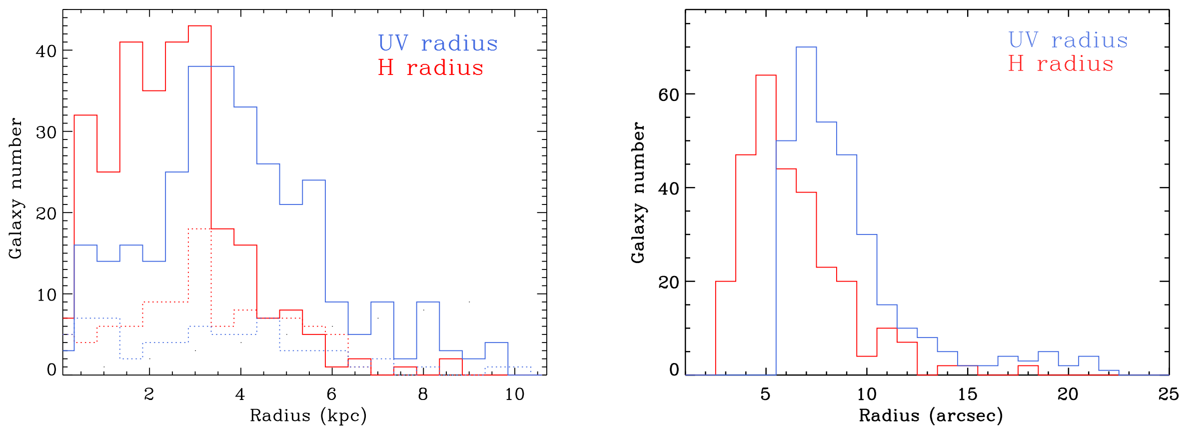

Fig. 3 *Left panel:* Histogram of the radius measurement results. We show the FUV radius in blue and the H band radius in red. The dotted lines trace the histogram of the radius upper limits for the targets not resolved in FUV or H band images. *Right panel:* Histogram of the de-convolved radius in the unit of arcsec. Most of our targets have size larger than the image resolution.

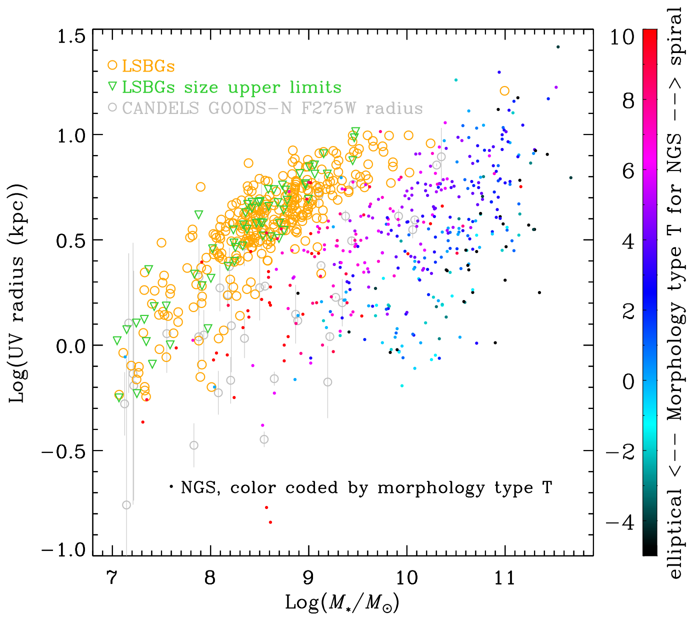

Fig. 4 The FUV radius vs. the stellar mass of this LSBG sample (*orange open circles* for FUV resolved sample and *green triangles* for the size upper limits of the unresolved FUV sample) and the GALEX Nearby Galaxies Survey (NGS, at z ~0 Gil de Paz et al. 2007) results (*filled circles*, colour coded by the morphology type). We also include the HST F275W band half-light radius galaxies at $0.05 < Z < 0.3$ from the CANDELS GOODS-N field (Cheng et al. 2020) (*grey open circles*). Our LSBG sample FUV radii are 0.5 dex larger than those of the CANDELS sample, and have a similar FUV radius as the local galaxies, but lower stellar mass.

10^{12}) at a similar redshift range as our LSBG sample ($z < 0.09$). Although the mass size relation has different branches for elliptical and disk galaxies (van der Wel et al. 2014), the LSBG sample mainly has stellar mass of about $10^{7.5} - 10^{9.5} M_{\odot}$, which is the stellar mass range of the local dwarf and disk galaxies in Trujillo et al. (2020). Our LSBG H band radii as a low mass disk galaxy sample (Du et al. 2019) show a consistent mass size distribution with the results of Trujillo et al. (2020).

We also display the CANDELS W160W band radius from Cheng et al. (2020) in Figure 5 by blue open circles. CANDELS results have one order of magnitude higher spatial resolution than the ground-based telescope images and much deeper image limiting magnitude. Therefore, the CANDELS survey can enable us to measure the radii of low mass galaxies that are not resolved in the SDSS image. The H band size-mass relation of the CANDELS results indeed shows a larger scatter with lower H band radius,

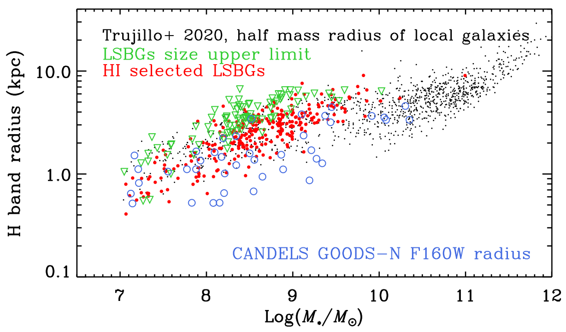

Fig. 5 The H band mass size relation of our LSBG sample. We also show the stellar mass vs. half-mass radius of 1005 low redshift ($z < 0.09$) galaxies selected from SDSS as a comparison (Trujillo et al. 2020). Moreover, we display the CANDELS results from Cheng et al. (2020) in blue open circles. CANDELS images enable us to measure the radii of low mass galaxies that are not spatially resolved in SDSS images.

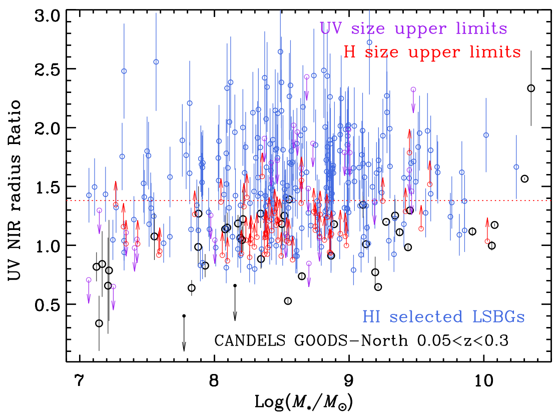

Fig. 6 The FUV-NIR radius ratio as a function of stellar mass for the LSBG sample (*blue open circles*). We mark the upper and lower limits of the size ratio for the FUV or H band unresolved LSBGs. As a comparison, we display the FUV-NIR radius ratio of the CANDELS sample with open circles, taken from Cheng et al. (2020). The red dotted line delineates the results ratio from GAMA results, where the FUV radius is extrapolated from the radius from u, g, r, i, z, J, H, K band average radius. The ratios of LSBGs are consistent with the expectation from the SDSS galaxies results.

implying that the Trujillo et al. (2020) and our LSBGs H band size mass relation may bias the spatially resolved low mass galaxies.

We showcase the radius of the H and FUV band LSBGs in Figure 6. The red dotted line is the FUV and H band radius ratio based on the average radius in different bands (Kelvin et al. 2012). We depict our LSBG size ratio as blue circles. For the LSBGs only resolved in FUV band image (58 galaxies) or H band images (27 galaxies), we show the size ratio as upper and lower limits in Figure 6. Thirty-three galaxies with neither an FUV nor H band resolved image are not displayed in Figure 6. We can see that the majority of LSBGs have a relatively larger UV size, yielding the ongoing star formation that occurs at larger galaxy radii. We will discuss the effect of the upper limits on our conclusion in Section 5.2.

Our LSBG sample mainly has a larger FUV size than the H band with a large scatter at a stellar-mass range of about $10^{8.5}\,M_\odot$. Even in the stellar mass range of about $10^7\,M_\odot$, where our previous work purports that the galaxy may have an "outside-in" growth mode, the LSBGs still have a more extended star formation size. The FUV and H band size of LSBGs indicate that the LSBGs have a similar stellar mass distribution as the other low mass galaxies, yet the ongoing star formation is more extended.

For an exponential disk, the central surface brightness (μ_0) and efficient brightness ($\mu_{\rm eff} = {\rm mag} + 2.5\log(\pi r_{\rm eff})$) have a relation that $\mu_0 = \mu_{\rm eff} - 1.83$ (Greco et al. 2018b). So, the LSBGs selected should have a larger B band radius, yielding a larger radius in the blue band.

The tight correlation between HI gas mass and size can help us to estimate the HI radius (Wang et al. 2016; Stevens et al. 2019). The HI mass of our LSBG sample is derived from $M_{\rm HI} = 2.35 \times 10^5 D^2 F_{\rm HI}$, where D is the target distance in the unit of Mpc and $F_{\rm HI}$ is the HI flux in the unit of Jy km s^2. We estimate the HI size by log(Diameter) = $(\log(M_{\rm HI}) - 6.54)/1.95$ (Graham 2013). Figure 8 features the result of HI and H band size as a function of FUV radius. The HI size is typically three times larger than the FUV radius, while the H band radius is about half the FUV radius.

5 DISCUSSION

We discuss the bias of our sample selection, radius of the LSBG population and the possible origin of the LSBG size in this section.

5.1 Bias of Our Sample Selection

There are a total of 544 targets with both GALEX and NIR observation coverage. To have a better measurement, we remove the 154 galaxies with close counterparts or galaxies located at the edge of either GALEX or NIR images, which would not bias our main results. We also remove the nine galaxies with both GALEX and NIR observations, but which have non-detection (5σ) in either band. The non-detection may be caused by dust extinction in UV bands, or shallow survey depth. Since the whole sample we used in this work contains 381 galaxies, much larger than the amount of the non-detection galaxies, we conclude that the removal of non-detections would not affect our results.

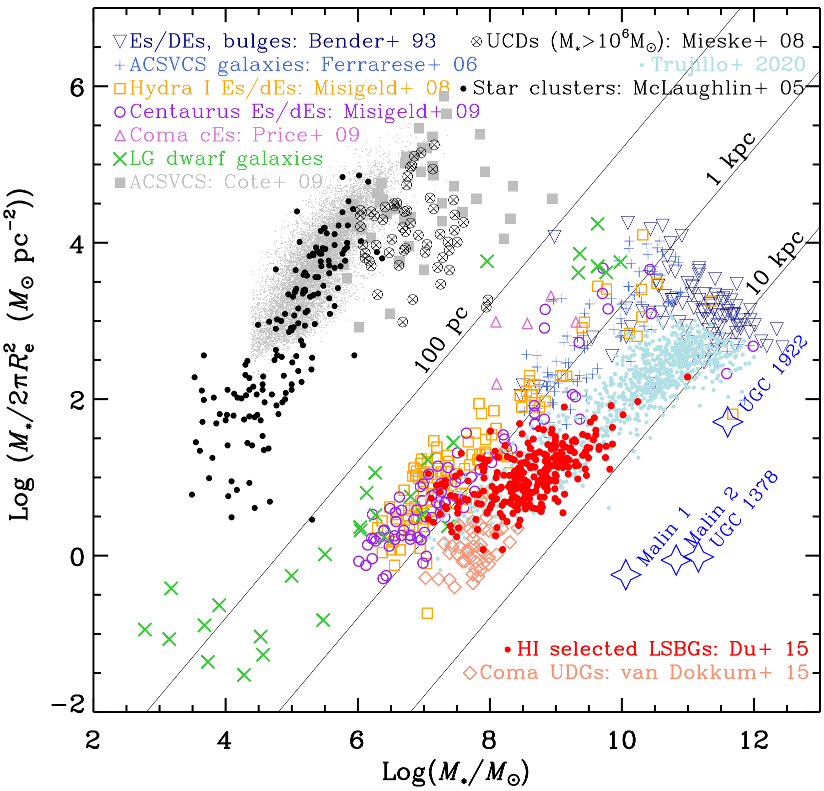

Fig. 7 The stellar mass and mass density distribution of the different stellar systems. This figure includes the sample introduced in Misgeld & Hilker (2011). We label the sample with references. We add the sample of Coma UDGs (van Dokkum et al. 2015, pink dimonds), low redshift galaxies (Trujillo et al. 2020, small blue dots) and the sample in this work (*red filled circles*). We also show the results of giant LSBGs such as Marlin 1 (Galaz et al. 2015), Marlin 2 (Kasparova et al. 2014), UGC 1922 (Saburova et al. 2018) and UGC 1378 (Saburova et al. 2019) in *open blue stars*. We demarcate the division line of compact stellar systems (*thick line* labeled by 100 pc), and the position of the stellar system with 1 kpc and 10 kpc size. Our sample mainly has similar radii as the massive galaxies and UDG sample.

5.2 Effect of the Size Limits

Our results affirm that most of the HI-selected LSBGs have a more extended FUV size than the H band. This conclusion still holds for the H band unresolved galaxies. LSBGs in our sample with an FUV unresolved image (a total of 60 galaxies) would be candidates for the LSBG compact star formation cores (Cheng et al. 2020), but still need more data to constrain the star formation region (e.g., Hα narrow band observation).

5.3 Size of the LSBG Population

Figures 4 and 5 demonstrate the size of the LSBGs in FUV and H band. The consistent distribution of the H band mass size relation in Figure 5 roughly indicates that the LSBGs are not exceptional in terms of stellar mass distribution. However, the differences between the LSBGs and other galaxies are clearly apparent in Figure 4, illustrating that LSBGs are typically 0.5 dex larger than the nearby galaxy sample. The magnitude and diameter limits of the GALEX NGS results yield an absence of the low surface brightness galaxy population (see Gil de Paz et al. 2007, for more details). Therefore, our LSBG sample complements the GALEX NGS results, and manifests larger radii than local high surface brightness galaxies.

The large scatter and the FUV size and the stellar mass distribution may be caused by complex dust extinction in massive galaxies, and the clumpy or irregular star formation morphology in low mass galaxies. Nevertheless, the LSBGs almost possess the largest FUV size at a fixed stellar mass range. Previous studies affirmed that the galaxy mass-size relation may correlate with galaxy properties such as morphology, Sérsic index, specific SFR, galaxy population and other factors (Fernández Lorenzo et al. 2013; Lange et al. 2015; Whitaker et al. 2017). We also signify the galaxy morphology by the colour bar in Figure 4. Although the scatter in the FUV size-stellar mass

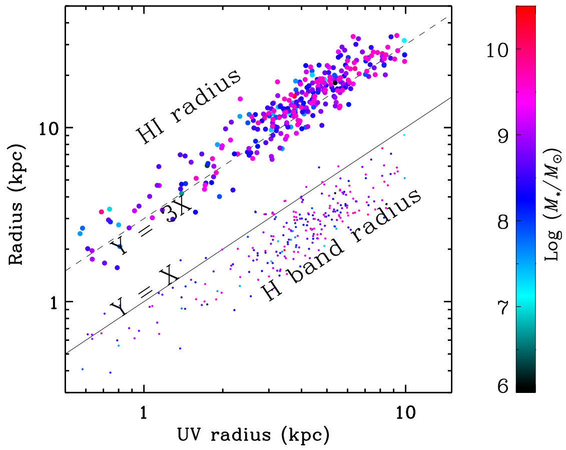

Fig. 8 The HI gas radii and H band radii vs. FUV radii for our LSBG sample. The HI radius is estimated from the HI size-mass relation (Wang et al. 2016), which is a very tight correlation along 5 orders of magnitude. We colour the sample by the stellar mass. The H band radius is 0.5 dex smaller than the FUV radius, while the HI gas is distributed at about 3 times larger radius.

relation is large, galaxies with a similar morphology still exhibit the trend that galaxies with the same morphology tend to have a tight correlation (Fernández Lorenzo et al. 2013). The location of LSBGs in Figure 4 implies a possible method to select LSBGs from the low mass, UV or U band disk galaxies. Current and future large field deep u band survey projects such as the Canada-France-Hawaii Telescope (CFHT) Large Area U-band Deep Survey (CLAUDS, Sawicki et al. 2019) or the u band data released by Rubin Observatory (LSST Science Collaboration et al. 2009; Brough et al. 2020) may be very helpful in selecting a large LSBG sample efficiently.

5.4 Stellar Mass Build Up of LSBGs

A low mass galaxy sample in Trujillo et al. (2020) is selected from BOSS results (Maraston et al. 2013) which should not mainly consist of LSBGs. The consistency of the distribution in Figure 5 indicates that the stars in LSBGs have already been assembled in other galaxies. However, Figure 4 affirms that the star-forming size of the LSBGs is about 0.5 dex larger than that of normal HSBGs, which is reasonable since the low surface brightness implies a larger radius. So, we can expect that the stellar mass would increase faster in the extended region of the LSBGs.

We show the stellar mass and mass density ($\Sigma_{M_*} = M_*/2\pi R_{\rm H}^2$) of our LSBG sample in a big picture of the different stellar systems over 10 orders of magnitude in mass (Misgeld & Hilker 2011; van Dokkum et al. 2015; Eigenthaler et al. 2018) in Figure 7[3]. The 100 pc line delineates the division between compact and extended stellar systems (Eigenthaler et al. 2018). The LSBG systems are located in between ultra-diffuse galaxies (UDGs) in the Coma galaxy cluster and massive galaxies, with about a similar magnitude of the radius. Definition of the UDGs in recent studies is $R_e > 1.5$ kpc and $\langle\mu(r, R_e)\rangle > 24$ mag arcsec^{-2}, which mainly have a lower surface brightness than our LSBG sample (see panel (d) of fig. 3 in Du et al. 2019), and lower stellar mass. Both UDGs and LSBGs are a diffuse galaxy population and have low star formation efficiency. The adjacent location of the UDGs and LSBGs may imply that, if the UDS can have a sustained baryon inflow from IGM, and continuous star formation, then the UDGs may evolve to LSBGs, otherwise the UDGs may fade into a very diffuse, faint galaxy that is below the detection limit. For UGDs in the Coma cluster, the massive dark matter halo may sweep out the baryons nearby more efficiently, cut out the UGDs' baryon supply, and quench or swallow the UDGs by ram pressure or merger (Peng et al. 2010b). Therefore, the dense environment may cut down the connection between UDGs and LSBGs. One recent field UDG sample (Barbosa et al. 2020) selected from the wide-field Southern Photometric Local Universe Survey (S-PLUS) project (Mendes de Oliveira et al. 2019) manifests a typical stellar-mass of about $10^8\ M_\odot$ and radius of about 2.5 kpc, corresponding to $\log(M_*/2\pi R_e^2)$ of about 0.4, agreeing with the UDG properties from the Coma galaxy cluster, implying that the origin of the diffuse nature in UDG may not only be caused by the environment.

For a stellar mass of about $10^9\ M_\odot$, the HI selected LSBGs and low-z sample from Trujillo et al. (2020) in Figure 7 have lower mass density than elliptical galaxies, or the galaxy bulge, implying that the low mass sample in Trujillo et al. (2020) is mainly disk galaxies with no or weak central bulge structure. So, the consistency in the stellar mass vs. H band size relation also indicates that the stellar mass structure of LSBGs is similar to the low mass disk galaxies.

The current star formation in LSBGs would build stars at a larger radius (Fig. 4), thus the LSBGs would evolve into an extended disk galaxy with higher stellar mass, such as giant LSBGs like Marlin 1 (Galaz et al. 2015), Marlin 2 (Kasparova et al. 2014), UGC 1922 (Saburova et al. 2018) and UGC 1378 (Saburova et al. 2019) in Figure 7. Simulations of low-z diffuse galaxy formation also reveal the stellar disk flattening caused by supernova feedback (Di Cintio et al. 2017, 2019; Jiang et al. 2019). Then the evolution trace of LSBGs would go toward the right lower direction in Figure 7, where there may be some Giant

[3] The R_e in Figure 7 is measured from optical images. The difference in galaxy sizes measured from H band and r band is less than 0.2 dex (e.g., Kelvin et al. 2012).

LSBGs. The upper panel of Figure 5 also demonstrates that galaxies with stellar mass of about $10^{10}\ M_\odot$ ($\sim$ 1 dex higher than our sample) do not show a larger size. Thus we conclude that compaction might be necessary for the LSBGs (Tacchella et al. 2016) to evolve into massive high surface brightness galaxies.

5.5 Size of the HI Gas and the Star Formation Activity

The scale relation between the galaxy luminosity, surface brightness and Sérsic index shows that LSBGs tend to have flat morphology (Graham 2013, 2019), which can be represented as an exponential disk. If the gas in LSBG follows the distribution: $\Sigma_{\rm gas} = \Sigma_0 e^{-r/r_s}$, where the half light radius is about $R_e = 1.678 r_s$ (Peng et al. 2010a), if we simply adopt the Kennicutt-Schmidt law, the star formation disk would have $\Sigma_{\rm SFR} = A\Sigma_0 e^{-1.4\times r/r_s} = A\Sigma_0 e^{-r/(r_s/1.4)}$. Then the half light radius of star formation would be 1.4 times smaller than the gas radius. Figure 8 plots the sizes of FUV and HI, which are approximately the SFR and gas radius, and about 3 times the difference. So, the Kennicutt-Schmidt law might have an index of about 3 for LSBGs. Given that the range of the gas surface density in our LSBGs sample is small (Du et al. 2015), the steep slope indicates that a small change in the gas surface density would alter the star formation surface brightness a lot, so a steep slope for LSBG would lead to a large scatter (or not) in the Kennicutt-Schmidt relation in LSBGs.

5.5.1 *Theoretical implication*

Theoretical works (Mo et al. 1998; Amorisco & Loeb 2016; Peng & Renzini 2020) and recent simulations purport that large sized field galaxies may be located in the dark matter halo with high angular momentum (Liao et al. 2019; Martin et al. 2019; Tremmel et al. 2020). High rotation velocity will keep the baryons at a larger radius, and thus flatten the stellar distribution. Nevertheless, the formation of H_2 from HI gas requires high gas surface density and dust (Leroy et al. 2008). For our HI selected LSBG sample, the large size leads to a low HI surface density. So, the LSBGs would still lack H_2. Therefore, from a theoretical point of view, galaxies with large radii, such as LSBGs, should have a low SFR (Lei et al. 2018). Moreover, the high gas angular momentum would lead to a large gas size and even quench the galaxy by preventing gas inflow (Peng & Renzini 2020). Therefore, if the large FUV size of the LSBG is caused by large gas angular momentum, we would expect the LSBGs to be quenched into red, extended galaxies, such as the red LSBGs revealed by the HSC survey (Greco et al. 2018a).

6 CONCLUSIONS

We study the size of an HI-selected LSBG sample. Taking advantage of the low dust extinction in LSBGs, we utilize the UV image to represent the star formation distribution. We also use the H band image to trace the stellar mass distribution. We find the star-forming size of the LSBG is about 0.5 dex larger than the H band radius, so the star-forming activity in the LSBGs is still extended, rather than compact star-forming cores (Cheng et al. 2020). The H band radius is consistent with low-z disk galaxies, so LSBGs may have a similar stellar structure, but much larger ongoing star formation region. The star-forming size and stellar mass of the LSBGs imply that the deep and wide-field blue band images may help us to select a large LSBG sample efficiently. The HI size of LSBGs is about 3 times larger than the FUV, implying a steeper slope (or not) in the Kennicutt-Schmidt relation. We also discuss the possible link of UDGs and our LSBGs and formation path of the LSBGs.

Acknowledgements We thank the referee for carefully reading and providing constructive comments. C.C. is supported by the National Key R&D Program of China (Grant 2017YFA0402704) and by the National Natural Science Foundation of China (NSFC, Nos. 11803044, 11933003, 11673028). This work is sponsored (in part) by the Chinese Academy of Sciences (CAS), through a grant to the CAS South America Center for Astronomy (CASSACA). D.W. is also supported by the NSFC (Nos. U1931109 and 11733006), the Young Researcher Grant funded by National Astronomical Observatories, Chinese Academy of Sciences (CAS) and the Youth Innovation Promotion Association, CAS.

References

Amorisco, N. C., & Loeb, A. 2016, MNRAS, 459, L51
Barbosa, C. E., Zaritsky, D., Donnerstein, R., et al. 2020, ApJS, 247, 46
Barro, G., Pérez-González, P. G., Cava, A., et al. 2019, ApJS, 243, 22
Bothun, G., Impey, C., & McGaugh, S. 1997, PASP, 109, 745
Brough, S., Collins, C., Demarco, R., et al. 2020, arXiv e-prints, arXiv:2001.11067
Bruzual, G., & Charlot, S. 2003, MNRAS, 344, 1000
Calzetti, D., Armus, L., Bohlin, R. C., et al. 2000, ApJ, 533, 682
Cao, T.-W., Wu, H., Du, W., et al. 2017, AJ, 154, 116
Chabrier, G. 2003, PASP, 115, 763
Cheng, C., Xu, C. K., Xie, L., et al. 2020, A&A, 633, A105
Di Cintio, A., Brook, C. B., Dutton, A. A., et al. 2017, MNRAS, 466, L1
Di Cintio, A., Brook, C. B., Macciò, A. V., et al. 2019, MNRAS, 486, 2535
Du, W., Cheng, C., Wu, H., et al. 2019, MNRAS, 483, 1754

Du, W., Cheng, C., Zheng, Z., et al. 2020, AJ, 159, 138
Du, W., Wu, H., Lam, M. I., et al. 2015, AJ, 149, 199
Du, W., Wu, H., Zhu, Y., et al. 2017, ApJ, 837, 152
Eigenthaler, P., Puzia, T. H., Taylor, M. A., et al. 2018, ApJ, 855, 142
Fernández Lorenzo, M., Sulentic, J., Verdes-Montenegro, L., et al. 2013, MNRAS, 434, 325
Galaz, G., Milovic, C., Suc, V., et al. 2015, ApJL, 815, L29
Gil de Paz, A., Boissier, S., Madore, B. F., et al. 2007, ApJS, 173, 185
Glover, S. C. O., & Clark, P. C. 2012, MNRAS, 426, 377
Graham, A. W. 2013, Elliptical and Disk Galaxy Structure and Modern Scaling Laws, eds. T. D. Oswalt, & W. C. Keel, 6, Planets, Stars and Stellar Systems, 6: Extragalactic Astronomy and Cosmology (Springer Science+Business Media Dordrecht), 91
Graham, A. W. 2019, PASA, 36, e035
Greco, J. P., Goulding, A. D., Greene, J. E., et al. 2018a, ApJ, 866, 112
Greco, J. P., Greene, J. E., Strauss, M. A., et al. 2018b, ApJ, 857, 104
Grogin, N. A., Kocevski, D. D., Faber, S. M., et al. 2011, ApJS, 197, 35
Haynes, M. P., Giovanelli, R., Martin, A. M., et al. 2011, AJ, 142, 170
Haynes, M. P., Giovanelli, R., Kent, B. R., et al. 2018, ApJ, 861, 49
He, M., Wu, H., Du, W., et al. 2019, ApJ, 880, 30
Hollenbach, D., & McKee, C. F. 1979, ApJS, 41, 555
Huang, S., Haynes, M. P., Giovanelli, R., et al. 2012, ApJ, 756, 113
Impey, C., & Bothun, G. 1997, ARA&A, 35, 267
Jiang, F., Dekel, A., Freundlich, J., et al. 2019, MNRAS, 487, 5272
Kasparova, A. V., Saburova, A. S., Katkov, I. Y., et al. 2014, MNRAS, 437, 3072
Kelvin, L. S., Driver, S. P., Robotham, A. S. G., et al. 2012, MNRAS, 421, 1007
Kennicutt, Robert C., J. 1998, ARA&A, 36, 189
Kennicutt, R. C., & Evans, N. J. 2012, ARA&A, 50, 531
Koekemoer, A. M., Faber, S. M., Ferguson, H. C., et al. 2011, ApJS, 197, 36
Kriek, M., van Dokkum, P. G., Labbé, I., et al. 2009, ApJ, 700, 221
Lange, R., Driver, S. P., Robotham, A. S. G., et al. 2015, MNRAS, 447, 2603
Lei, F.-J., Wu, H., Zhu, Y.-N., et al. 2019, ApJS, 242, 11
Lei, F.-J., Wu, H., Du, W., et al. 2018, ApJS, 235, 18
Leroy, A. K., Walter, F., Brinks, E., et al. 2008, AJ, 136, 2782
Leroy, A. K., Sandstrom, K. M., Lang, D., et al. 2019, ApJS, 244, 24
Liao, S., Gao, L., Frenk, C. S., et al. 2019, MNRAS, 490, 5182
LSST Science Collaboration, Abell, P. A., Allison, J., et al. 2009, arXiv e-prints, arXiv:0912.0201
Maddox, N., Hess, K. M., Obreschkow, D., Jarvis, M. J., & Blyth, S. L. 2015, MNRAS, 447, 1610
Maraston, C., Pforr, J., Henriques, B. M., et al. 2013, MNRAS, 435, 2764
Martin, G., Kaviraj, S., Laigle, C., et al. 2019, MNRAS, 485, 796
McGaugh, S. S. 1996, MNRAS, 280, 337
Mendes de Oliveira, C., Ribeiro, T., Schoenell, W., et al. 2019, MNRAS, 489, 241
Misgeld, I., & Hilker, M. 2011, MNRAS, 414, 3699
Mo, H. J., Mao, S., & White, S. D. M. 1998, MNRAS, 295, 319
Oesch, P. A., Montes, M., Reddy, N., et al. 2018, ApJS, 237, 12
Oke, J. B., & Gunn, J. E. 1983, ApJ, 266, 713
Omukai, K., Tsuribe, T., Schneider, R., & Ferrara, A. 2005, ApJ, 626, 627
Peng, C. Y., Ho, L. C., Impey, C. D., et al. 2002, AJ, 124, 266
Peng, C. Y., Ho, L. C., Impey, C. D., et al. 2010a, AJ, 139, 2097
Peng, Y.-j., & Renzini, A. 2020, MNRAS, 491, L51
Peng, Y.-j., Lilly, S. J., Kovač, K., et al. 2010b, ApJ, 721, 193
Saburova, A. S., Chilingarian, I. V., Kasparova, A. V., et al. 2019, MNRAS, 489, 4669
Saburova, A. S., Chilingarian, I. V., Katkov, I. Y., et al. 2018, MNRAS, 481, 3534
Sawicki, M., Arnouts, S., Huang, J., et al. 2019, MNRAS, 489, 5202
Smith, J. A., Tucker, D. L., Kent, S., et al. 2002, AJ, 123, 2121
Stevens, A. R. H., Diemer, B., Lagos, C. d. P., et al. 2019, MNRAS, 490, 96
Suess, K. A., Kriek, M., Price, S. H., et al. 2019a, ApJ, 877, 103
Suess, K. A., Kriek, M., Price, S. H., et al. 2019b, ApJL, 885, L22
Tacchella, S., Dekel, A., Carollo, C. M., et al. 2016, MNRAS, 457, 2790
Tremmel, M., Wright, A. C., Brooks, A. M., et al. 2020, MNRAS, 497, 2786
Trujillo, I., Chamba, N., & Knapen, J. H. 2020, MNRAS, 493, 87
van der Wel, A., Franx, M., van Dokkum, P. G., et al. 2014, ApJ, 788, 28
van Dokkum, P. G., Abraham, R., Merritt, A., et al. 2015, ApJL, 798, L45
Wang, J., Koribalski, B. S., Serra, P., et al. 2016, MNRAS, 460, 2143
Whitaker, K. E., Bezanson, R., van Dokkum, P. G., et al. 2017, ApJ, 838, 19